Supplemental Material for: Electrically Tunable Valley Dynamics in Twisted WSe_2/WSe_2 Bilayers

Giovanni Scuri[1]*, Trond I. Andersen[1]*, You Zhou[1,2]*, Dominik S. Wild[1], Jiho Sung[1,2], Ryan J. Gelly[1], Damien Bérubé[3], Hoseok Heo[1,2], Linbo Shao[4], Andrew Y. Joe[1], Andrés M. Mier Valdivia[4], Takashi Taniguchi[5], Kenji Watanabe[5], Marko Lončar[4], Philip Kim[1,4], Mikhail D. Lukin[1]†, and Hongkun Park[1,2]†

[1]Department of Physics and [2]Department of Chemistry and Chemical Biology, Harvard University, Cambridge, Massachusetts 02138, USA

[3]Department of Physics, California Institute of Technology, Pasadena, California 91125, USA

[4]John A. Paulson School of Engineering and Applied Sciences, Harvard University, Cambridge, Massachusetts 02138, USA

[5]National Institute for Materials Science, 1-1 Namiki, Tsukuba 305-0044, Japan

*These authors contributed equally to this work.

†To whom correspondence should be addressed: hongkun_park@harvard.edu, lukin@physics.harvard.edu

I. MATERIALS AND METHODS

Flakes of hBN, graphene and WSe_2 were mechanically exfoliated from bulk crystals onto Si wafers (with 285 nm SiO_2). Monolayer and bilayer WSe_2 were identified using optical microscopy and later confirmed in photoluminescence measurements. The thicknesses of hBN flakes were determined with atomic force microscopy. The heterostructures were then assembled with the dry-transfer method, using the tear-and-stack technique [1,2] to form twisted bilayer WSe_2. Next, electrical contacts to the WSe_2 and graphite gates were defined with electron-beam lithography and deposited through thermal evaporation (10 nm Cr+90 nm Au). Optical measurements were conducted in a 4 K cryostat (Montana Instruments), using a self-built confocal setup with an 0.75 NA objective. The DOCP was measured with two polarizers in the excitation and collection paths, and a quarter wave plate directly above the objective. To eliminate any polarization-dependent instrument response, all DOCP measurements included excitation with (and collection of) both σ_+ and σ_- light. PL measurements were carried out using a 660 nm diode laser. A sub-picosecond pulsed laser (Coherent) and a streak camera (Hamamatsu) were used in the time-resolved PL measurements.

II. EXCITON CHARACTERIZATION BASED ON DC STARK SHIFT

Upon applying a vertical electric field, excitons experience a Stark shift given by $\Delta E = E_z \cdot e \cdot d$, where E is the exciton energy, E_z is the applied electric field, d is the (vertical) electron-hole separation, and e is the elementary charge. Since interlayer excitons have an out-of-plane dipole moment (d), unlike intralayer excitons, the two species can be distinguished through electric field dependent PL measurements (Fig. 2(a) and Fig. S2). In all of our devices, the higher-energy feature (~ 1.7 eV) exhibits no Stark shift, and is therefore attributed to intralayer excitons. The lower-

energy peaks, on the other hand, show a clear shift, and are therefore assigned to interlayer excitons.

The interlayer excitons are expected to be momentum indirect, because their PL energy is lower than that of the direct intralayer exciton, even with their weaker binding energy [3]. This is further supported by the fact that the extracted electron-hole separation, $d = 0.37$ nm (0.36 nm in 2° twist device), is significantly smaller than the full interlayer separation ($d_0 \sim 0.6$ nm) [3] that would be expected if both carriers were at the K point. It is also not consistent with the Γ-K transition, because the wavefunction at the Γ-point is completely delocalized between the two layers [4,5], causing $d \sim d_0/2$. Instead, the extracted electron-hole separation is consistent with the K to Q transition, where the hole is localized in a single layer and the electron is partially delocalized [6].

III. SPATIAL DEPENDENCE OF DOCP IN A SAMPLE CONTAINING BOTH NATURAL AND TWISTED BILAYER REGIONS

To confirm the stark contrast in DOCP between natural and twisted bilayer WSe_2, we fabricate an hBN-encapsulated TMD heterostructure that contains both natural (180°) and twisted (~0°) bilayer regions (Fig. S3(a)). The device was made from a single exfoliated WSe_2 flake that had both a bilayer and a monolayer region, the latter of which was torn and stacked on top of itself. Integrating only the interlayer exciton emission (photon energies below 1.6 eV), we find that the natural bilayer area exhibits almost no DOCP, while the twisted region has a DOCP close to 50% almost everywhere, except in sporadic defect spots (Fig. S3(b)).

IV. FITTING OF LIFETIME DATA

To fit the full time-dependence of the photoluminescence in the intrinsic regime, we use a biexponential decay convoluted with the system response, $s(t)$, as measured from the response of our sub-picosecond laser:

$$p(t) = \left(A_1 e^{-t/\tau_1} + A_2 e^{-t/\tau_2}\right) * s(t - t_0).$$

Here, τ_1 and τ_2 are the fast and slow decay timescales, with corresponding amplitudes A_1 and A_2. This model is used for both the co- and cross-polarized emission components (with separate fit parameters), and t_0 accounts for the observed delay between the two. The fits are shown as dotted lines in Fig. 3(a), with corresponding DOCP in Fig. 3(d).

In the *n*- and *p*-doped regimes, we focus on shorter timescales due to their shorter exciton and valley lifetimes, respectively. At these timescales, we only observe a single exponential decay and therefore fit with a linear coupled model, which also allows for extracting the valley lifetime, τ_v:

$$\dot{p}_\mathrm{co} = -\frac{p_\mathrm{co}}{\tau_1} - \frac{p_\mathrm{co} - p_\mathrm{cross}}{\tau_\mathrm{v}} + (1 - \alpha) \cdot s(t),$$

$$\dot{p}_\mathrm{cross} = -\frac{p_\mathrm{cross}}{\tau_1} - \frac{p_\mathrm{cross} - p_\mathrm{co}}{\tau_\mathrm{v}} + \alpha \cdot s(t).$$

Here, p_co and p_cross are the co- and cross-polarized exciton populations, and α is the proportion of cross-polarized excitons due to imperfect excitation. In order to account for the system response, we use the measured laser pulse, $s(t)$, as the laser input. The fits and corresponding DOCP are shown with dashed lines in Fig. 3(b)-(d). This model was also used for fitting in the intrinsic regime at longer timescales (inset of Fig. 3(d)).

V. INTRA- AND INTERLAYER *K*-*Q* EXCITONS

The wavefunction at the *Q*-point in twisted bilayer WSe_2 is expected to be more layer delocalized than that at the *K*-point, but still not fully delocalized as in the case of natural bilayers (Fig. S6(a)). Hence, there are two candidate *K*-*Q* exciton species: the intralayer species, where the electron wavefunction is more localized in the same layer as the hole (Fig. S6(b)), and the interlayer species where the electron is more localized in the opposite layer (Fig. S6(c)). The intra- (inter-) layer *K*-*Q* exciton is expected to exhibit an electron-hole separation that is smaller (greater) than $\frac{d_o}{2} \sim 0.3$ nm. Thus, the extracted electron-hole separation of 0.37 nm in our work indicates that the interlayer *K*-*Q* exciton dominates in PL. In this section, we explain why this is also to be expected theoretically.

Crucially, the bands are not layer degenerate in twisted bilayers, even at zero electric field. This important difference from natural bilayers arises from the broken inversion symmetry, and is most easily understood by starting from the limit of zero twist angle, i.e. AB (3R) stacking. In that case, the W-atoms in the top layer are vertically aligned with Se-atoms in the other layer, while the W-atoms in the bottom layer are not. This difference in atomic environment renders the bands non-degenerate between the two layers, as shown both theoretically (Refs. [6-8]) and experimentally (Ref. [9]). In particular, theoretical studies suggest that the lowest conduction band at the *Q*-point and the highest valence band at the *K*-point are preferentially localized in opposite layers, thus promoting the interlayer species. Our observations suggest that this effect is stronger than the difference in binding energy between the intra- and interlayer *K*-*Q* species, thus causing the interlayer exciton to be the lowest energy state.

Proceeding to non-zero twist angles, the system now exhibits a smooth periodic variation between AB- and BA-stacked points (the moiré pattern), and at large twist angles, the wavefunctions

become delocalized over multiple moiré cells. Nevertheless, as shown in Refs. [10,11], the delocalized hole wavefunction of the highest band at the *K*-point is still concentrated near the AB(BA)-stacked sites in the bottom (top) layer. Conversely, the lowest CB *Q*-bands are expected to be preferentially concentrated near the BA(AB)-stacked sites in the bottom (top) layer. Since the intralayer exciton consists of an electron and hole that are concentrated in different parts of the sublattice, the wavefunction overlap is very small (Fig. S6(b)). In the case of interlayer excitons, on the other hand, the electron is predicted to be in the same domain and layer as the hole almost 40% of the time (Fig. S6(c)) [6]. Hence, it is expected that the interlayer *K*-*Q* species has both higher binding energy and stronger oscillator strength than the intralayer counterpart, and is thus the exciton species responsible for the lower energy peaks observed in our experiment.

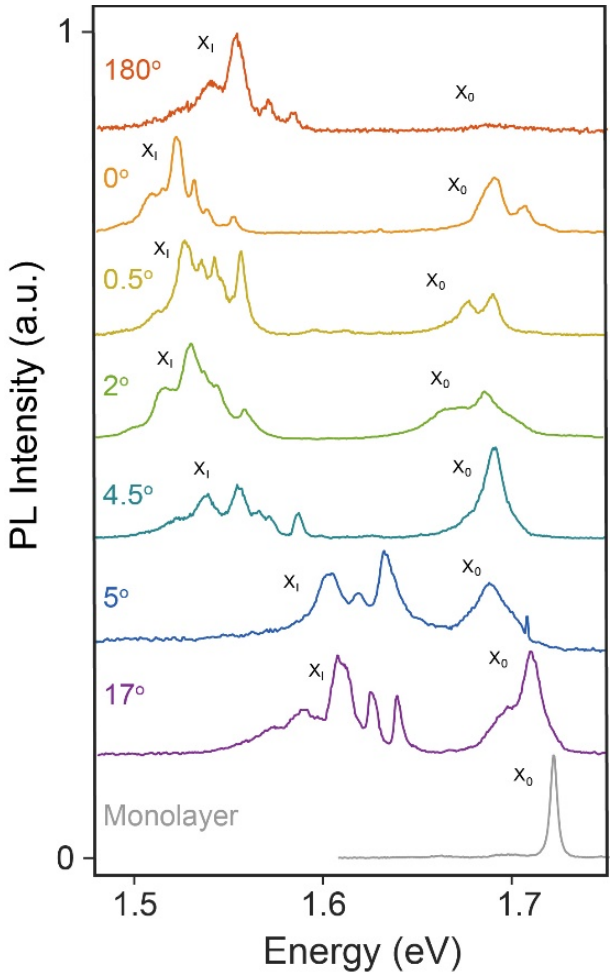

Fig. S1: Photoluminescence from additional samples. Colored (grey) curves show PL from bilayer (monolayer) WSe_2, including additional twist angles of 0.5°, 4.5° and 5° not displayed in the main text. The devices with 4.5° and 5° twist angles show the same interlayer exciton blue-shift as was presented for the 17° sample in the main text.

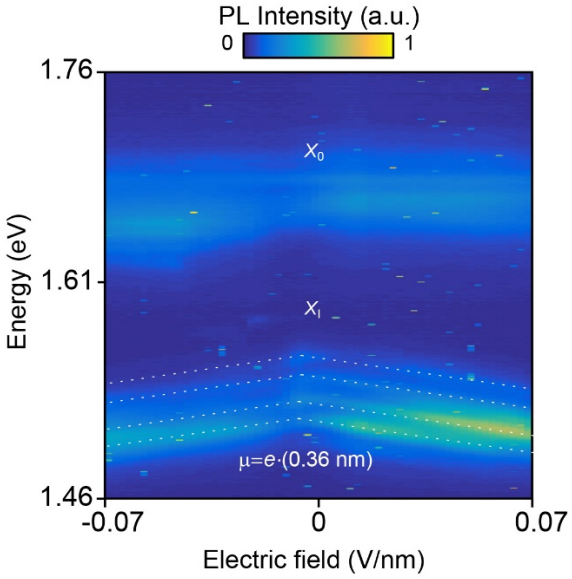

Fig. S2: Electric field dependence of PL in device with 2º twist angle. While the intralayer exciton (~ 1.7 eV) does not shift observably with electric field, the interlayer excitons ($\sim 1.5 - 1.6$ eV) exhibit a clear Stark shift (dashed white lines). The corresponding electron-hole separation is 0.36 nm, similar to the value extracted in the 17º device (0.37 nm).

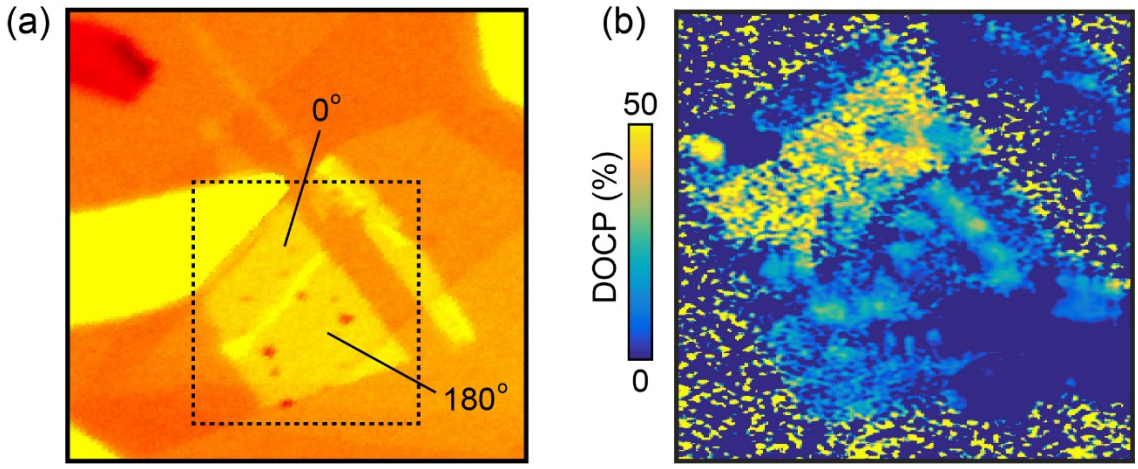

Fig. S3: Spatial map of DOCP. (a) Optical image of an hBN-encapsulated heterostructure that contains both natural (180º, lower right) and twisted (~0º, upper left) bilayer regions. (b) Spatial dependence of average interlayer exciton DOCP (photon energy below 1.6 eV). Consistent with PL spectra shown in the main text, the twisted bilayer region exhibits much higher DOCP than the natural bilayer region.

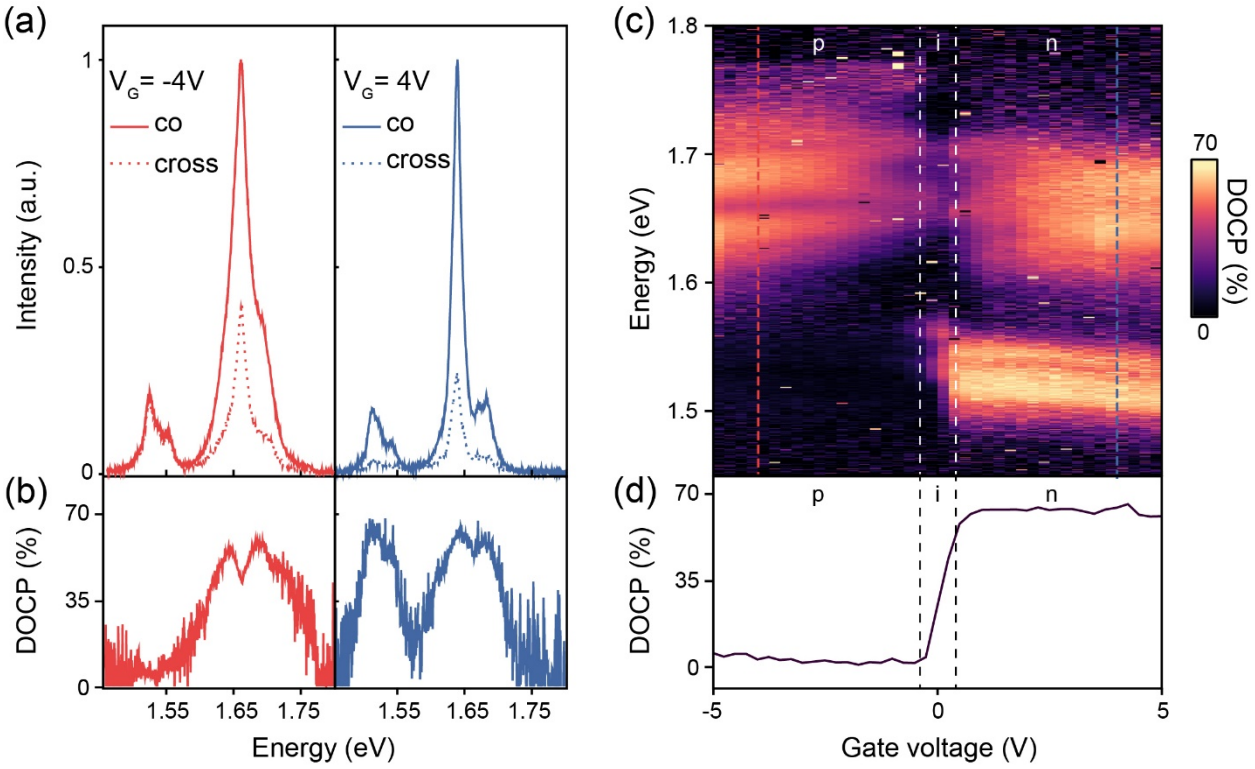

Fig. S4: Doping dependence of DOCP in device with 2º twist angle. (a) Polarization-resolved photoluminescence spectra from 2º-twisted bilayer WSe_2 at gate voltages V_G=-4 V (left) and V_G=4 V (right). Solid and dashed curves show co- and cross-polarized emission, respectively. (b) DOCP calculated from PL spectra in (a). As in the 17º device presented in the main text, the interlayer DOCP is much higher in the *n*-doped regime than in the *p*-doped regime. (c) Full gate dependence of DOCP. (d) DOCP of the brightest interlayer exciton peak as a function of gate voltage. Since this device exits the intrinsic regime at relatively low gate voltages, plateaus are only observed in the *p*- and *n*-doped regimes.

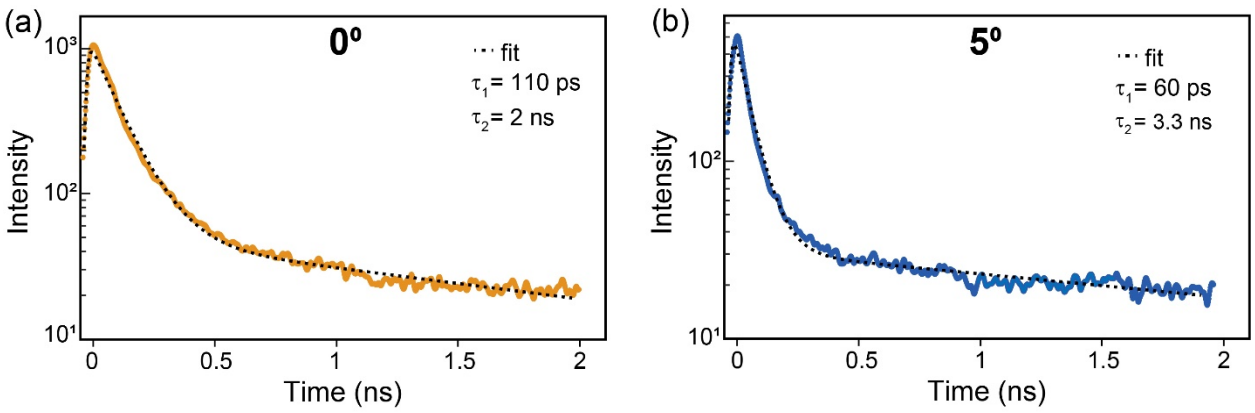

Fig. S5: Exciton lifetime in additional samples. (a)-(b) Time-resolved PL measurements from devices with 0º (a) and 5º (b) twist angles (colored dots). Dotted black lines are biexponential fits convoluted with the system response. The extracted fast and short timescales are τ_1=110 (60) ps and τ_2=2.0 (3.3) ns for the device with 0º (5º) twist angle.

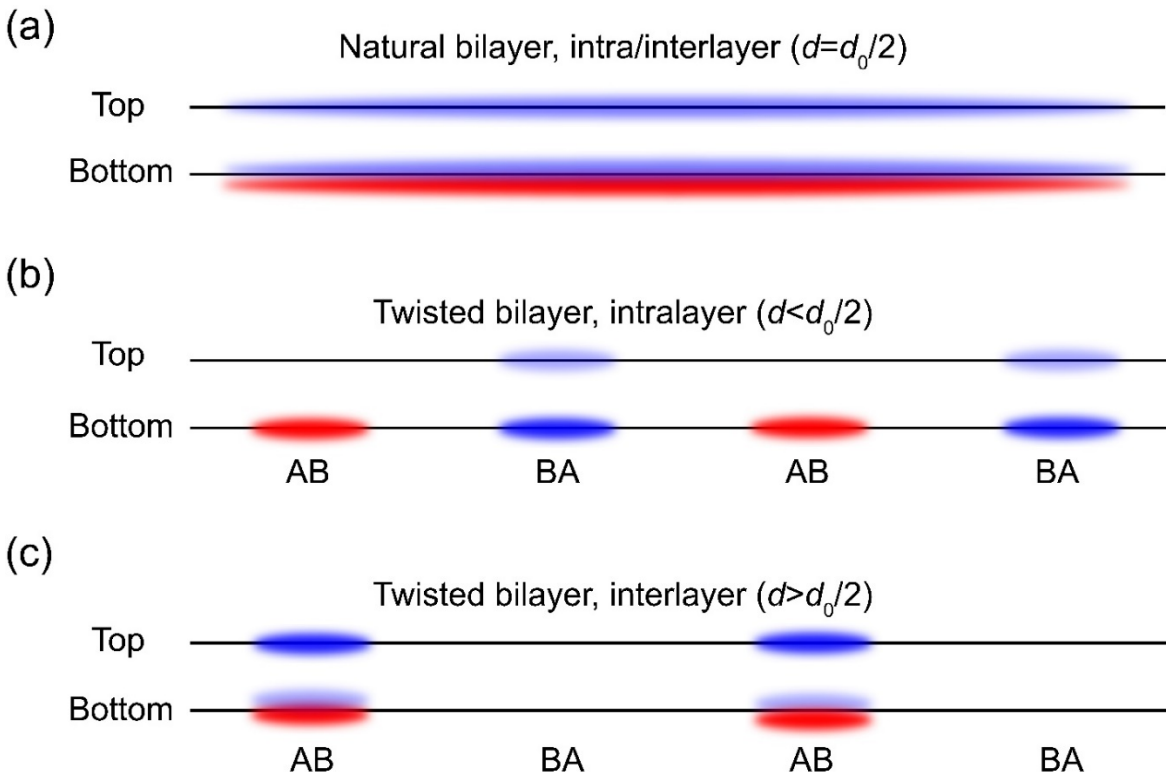

Fig. S6. Electron (blue, *Q*-point) and hole (red, *K*-point) wavefunctions in natural and twisted bilayers (only the bottom layer hole wavefunction is shown for simplicity). (a) In natural bilayers, the wavefunction at the *Q*-point is completely delocalized between the layers, causing the inter- and intralayer *K*-*Q* exciton to be equivalent. The expected electron-hole separation is half the interlayer spacing ($d = d_0/2$). (b)-(c) In twisted bilayers, the hole wavefunction is concentrated near the AB(BA)-stacked sites in the bottom (top) layer. In contrast, the electron wavefunction is preferentially concentrated near the BA(AB)-stacked sites in the bottom (top) layer. Thus, the electron-hole wavefunction overlap is expected to be larger for the interlayer exciton (c) than the intralayer exciton (b).

References:

[1] K. Kim *et al.*, van der Waals Heterostructures with High Accuracy Rotational Alignment, Nano Letters **16**, 1989 (2016).

[2] Y. Cao, V. Fatemi, S. Fang, K. Watanabe, T. Taniguchi, E. Kaxiras, and P. Jarillo-Herrero, Unconventional superconductivity in magic-angle graphene superlattices, Nature **556**, 43 (2018).

[3] L. A. Jauregui *et al.*, Electrical control of interlayer exciton dynamics in atomically thin heterostructures, Science **366**, 870 (2019).

[4] J. E. Padilha, H. Peelaers, A. Janotti, and C. G. Van de Walle, Nature and evolution of the band-edge states in MoS_2: From monolayer to bulk, Physical Review B **90**, 205420 (2014).

[5] A. M. van der Zande *et al.*, Tailoring the Electronic Structure in Bilayer Molybdenum Disulfide via Interlayer Twist, Nano Letters **14**, 3869 (2014).

[6] V. Enaldiev, V. Zólyomi, C. Yelgel, S. Magorrian, and V. Fal'ko, Stacking domains and dislocation networks in marginally twisted bilayers of transition metal dichalcogenides, arXiv:1911.12804 [Phys. Rev. Lett. (to be published)].

[7] W. Li, T. Wang, X. Dai, X. Wang, C. Zhai, Y. Ma, and S. Chang, Bandgap engineering of different stacking WS_2 bilayer under an external electric field, Solid State Communications **225**, 32 (2016).

[8] X. Fan, W. T. Zheng, J.-L. Kuo, D. J. Singh, C. Q. Sun, and W. Zhu, Modulation of electronic properties from stacking orders and spin-orbit coupling for 3R-type MoS_2, Scientific Reports **6**, 24140 (2016).

[9] A. Weston *et al.*, Atomic reconstruction in twisted bilayers of transition metal dichalcogenides, arXiv:1911.12664.

[10] H. Yu, M. Chen, and W. Yao, Giant magnetic field from moiré induced Berry phase in homobilayer semiconductors, National Science Review **7**, 12 (2020).

[11] F. Wu, T. Lovorn, E. Tutuc, I. Martin, and A. H. MacDonald, Topological Insulators in Twisted Transition Metal Dichalcogenide Homobilayers, Physical Review Letters **122**, 086402 (2019).